





# Crystal structures of a novel family IV esterase in free and substrate-bound form

Astrid Höppner<sup>1</sup>, Alexander Bollinger<sup>2</sup> , Stefanie Kobus<sup>1</sup>, Stephan Thies<sup>2</sup> ,  
 Cristina Coscolín<sup>3</sup> , Manuel Ferrer<sup>3</sup> , Karl-Erich Jaeger<sup>2</sup>  and Sander H. J. Smits<sup>1,4</sup> 

<sup>1</sup> Center for Structural Studies, Heinrich-Heine-University, Düsseldorf, Germany

<sup>2</sup> Institute of Molecular Enzyme Technology, Heinrich-Heine-University Düsseldorf, Jülich, Germany

<sup>3</sup> Institute of Catalysis, Consejo Superior de Investigaciones Científicas, Madrid, Spain

<sup>4</sup> Institute of Biochemistry, Heinrich-Heine-University, Düsseldorf, Germany

## Keywords

esterase; inhibitor-bound; metagenome;  
 substrate promiscuity;  $\alpha/\beta$ -fold hydrolase

## Correspondence

S. H. J. Smits, Institute of Biochemistry,  
 Heinrich-Heine-University, Universitätsstr. 1,  
 Düsseldorf D-40225, Germany  
 Tel: +49 211 81 12647  
 E-mail: sander.smits@hhu.de

Astrid Höppner and Alexander Bollinger  
 contributed equally to this study

(Received 9 October 2020, revised 26  
 November 2020, accepted 7 December  
 2020)

doi:10.1111/febs.15680

Bacterial lipolytic enzymes of family IV are homologs of the mammalian hormone-sensitive lipases (HSL) and have been successfully used for various biotechnological applications. The broad substrate specificity and ability for enantio-, regio-, and stereoselective hydrolysis are remarkable features of enzymes from this class. Many crystal structures are available for esterases and lipases, but structures of enzyme–substrate or enzyme–inhibitor complexes are less frequent although important to understand the molecular basis of enzyme–substrate interaction and to rationalize biochemical enzyme characteristics. Here, we report on the structures of a novel family IV esterase isolated from a metagenomic screen, which shows a broad substrate specificity. We solved the crystal structures in the apo form and with a bound substrate analogue at 1.35 and 1.81 Å resolution, respectively. This enzyme named PtEst1 hydrolyzed more than 60 out of 96 structurally different ester substrates thus being substrate promiscuous. Its broad substrate specificity is in accord with a large active site cavity, which is covered by an  $\alpha$ -helical cap domain. The substrate analogue methyl 4-methylumbelliferyl hexylphosphonate was rapidly hydrolyzed by the enzyme leading to a complete inactivation caused by covalent binding of phosphinic acid to the catalytic serine. Interestingly, the alcohol leaving group 4-methylumbelliferone was found remaining in the active site cavity, and additionally, a complete inhibitor molecule was found at the cap domain next to the entrance of the substrate tunnel. This unique situation allowed gaining valuable insights into the role of the cap domain for enzyme–substrate interaction of esterases belonging to family IV.

## Database

Structural data of PtEst1 are available in the worldwide protein data bank (<https://www.rcsb.org>) under the accession codes: 6Z68 (apo-PtEst1) and 6Z69 (PtEst1-inhibitor complex).

## Abbreviations

EPPS, 4-(2-Hydroxyethyl)-1-piperazinepropanesulfonic acid; HPA, hexyl(methoxy)phosphinic acid; HSL, hormone-sensitive lipases; IMAC, immobilized metal ion affinity chromatography; kDa, Kilo dalton; M4MHP, methyl 4-methylumbelliferyl hexylphosphonate; MUB, 4-methylumbelliferone; PEG, polyethylene glycol; pNPB, 4-nitrophenyl butyrate; rmsd, root-mean-square deviation; SEC, size exclusion chromatography; U, unit; v/v, volume/volume.

## Introduction

Lipolytic enzymes, that is, lipases and esterases, are among the most important biocatalysts in the field of biotechnology [1]. These enzymes catalyze the reversible hydrolysis of carboxylic esters, producing a carboxylic acid and an alcohol, and thus, they are classified by their function as carboxylic ester hydrolases (EC 3.1.1). Beyond this classification, bacterial lipolytic enzymes can be grouped according to their primary sequence into 19 different families [2]. The overall sequence identity among these enzymes is low, but they share specific conserved sequence motifs (e.g., the pentapeptide GX SXG, comprising the nucleophilic serine) owing to their common catalytic mechanism, which is composed of a nucleophile, acid, and base catalytic triad [3,4]. Despite their high sequence diversity, most enzymes of the carboxylic ester hydrolase class show a canonical  $\alpha/\beta$ -hydrolase fold, which is well explored by more than 1500 available protein structures according to the lipase engineering database [5]; only a few examples are known which show a  $\beta$ -propeller fold or an  $\alpha$ -helix bundle structure [6]. Important structural differences among  $\alpha/\beta$ -hydrolases are the presence of a lid or a cap domain, and the oxyanion hole signature [5]. Where lids are mobile elements, shielding the hydrophobic active site, effect interfacial activation, and influence substrate specificity [7], caps are reported to be immobile elements [5], confining the entrance to the enzyme's active site. The cap domain has been shown to be involved in the enzyme's thermostability [8] and taking part in substrate recognition [9]. The oxyanion hole is either build by the backbone amine of an amino acid next to a glycine (GX type), the last glycine of a triple glycine motif (GGGX type), or an amino acid with a large side chain (Y type) [5].

Despite the intensely studied catalytic mechanism based on a wealth of available structures for this class of enzymes, application relevant characteristics like a broad substrate range or selectivity for enantiomers are not completely understood. It was shown that a high number of substrate promiscuous ester hydrolases can be found among bacterial lipolytic enzymes of family IV [10]; however, the chiral selectivity of highly substrate promiscuous ester hydrolases was generally low. To understand such characteristics, insights into the enzyme–substrate interaction on a molecular level are needed. However, many structures lack a bound substrate analogue, which is a prerequisite to study distinct enzyme–substrate interactions. Here, we describe the identification of a novel carboxylic ester hydrolase, isolated from a metagenomics screen, with

an extraordinary broad substrate specificity and its crystal structure in the apo, as well as in substrate analogue bound form. The inhibitor-bound state shows the inhibitor hexyl(methoxy)phosphinic acid moiety covalently attached to the catalytic serine, while the 4-methylumbelliferone leaving group is still captured in the active site cavity. Moreover, a nonhydrolyzed ester methyl 4-methylumbelliferyl hexylphosphonate was found to be bound to the enzyme's cap domain. This unique situation gives novel insights into the enzyme–substrate interaction and the flexibility of the active site cavity for this important class of carboxylic ester hydrolases. The structural information contributes to a mechanistic understanding of the molecular basis for substrate recognition in cap domain comprising family IV esterases.

## Results

### Identification and heterologous expression of the novel metagenomic esterase *PtEst1*

Activity-based screening of a metagenomic library, which was enriched with cyclohexanol succinate as the sole carbon source, yielded one clone showing prominent esterase activity on tributyrin containing agar plates. The metagenomic DNA of this clone, Cyc\_TB025, was sequenced, and a gene, *PtEst1* (GenBank Accession No. MT942606), was identified, coding for a putative esterase. A BLAST search of the translated gene sequence against the NCBI nonredundant protein sequences database showed a high amino acid sequence identity (99%) to the  $\alpha/\beta$  hydrolase fold domain-containing protein WP\_073459097 of the actinomycete *Pseudonocardia thermophila*. Only one different amino acid was identified at position 271, which is valine in *PtEst1* and leucine in WP\_073459097. A multiple amino acid sequence alignment of *PtEst1* with proteins of different families of bacterial lipolytic enzymes [11] assigned the novel esterase to family IV according to the Arpigny and Jaeger classification [2]. For further analysis, the protein was produced as a C-terminal histidine-tag fusion protein with *Escherichia coli* LOBSTR [12] and purified by immobilized metal ion affinity chromatography (IMAC) and size exclusion chromatography (SEC), revealing a single band of about 40 kDa molecular weight, as determined by SDS/PAGE (Fig. 1).

### Biochemical characteristics

Many family IV bacterial esterases have been shown to be substrate promiscuous [10]. Hence, we performed

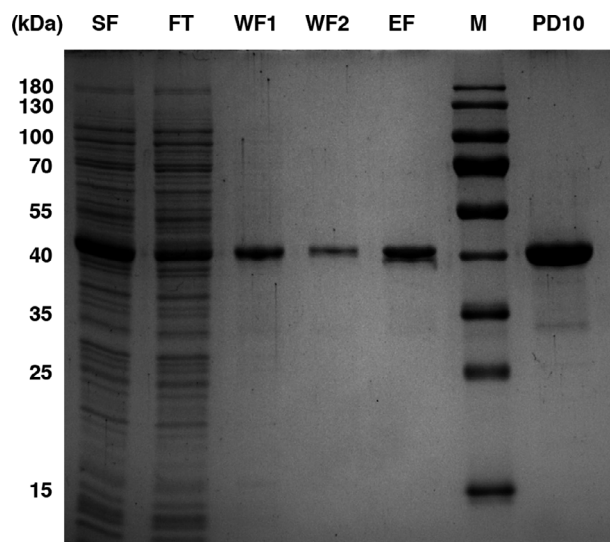


**Fig. 1.** Purification of PtEst1. Coomassie stained SDS/PAGE of the IMAC purification of PtEst1. Soluble proteins of the cell extract of the *Escherichia coli* LOBSTR expression culture (SF), unbound proteins of the IMAC (FT), proteins found in washing step 1 (WF1) and 2 (WF2), proteins eluted from the IMAC column (EF), and the purified protein after desalting (PD10) are shown. PageRuler prestained protein ladder was used as molecular weight standard (M).

a high-throughput substrate fingerprinting analysis with 96 structurally diverse ester substrates to rank the substrate spectrum of the novel esterase PtEst1. Indeed, we observed hydrolysis of 62 out of 96 esters, which classifies PtEst1 as prominent substrate promiscuous [10]. The highest activity was observed with small substrates featuring esters of ethanol with short fatty acids (e.g., 3-oxobutyrate, 3-oxohexanoate). Esters with aromatic or cyclic alcohol moieties (e.g., phenyl propionate, methyl mandelate, or cyclohexyl butyrate) were also converted fast, whereas esters with long carbon chains were converted less effective (e.g., methyl octanoate) or were not accepted at all (e.g., ethyl myristate or triolein) (Table 1).

In accordance with the cultivation at 50 °C during the enrichment process, preceding the metagenomic library construction, PtEst1 showed a half inactivation temperature of 55 °C (Fig. 2B). The pH optimum was determined at pH 7 (Fig. 2A). We also tested the tolerance of PtEst1 toward two of the most frequently applied polar solvents in industrial biocatalysis, methanol, and acetonitrile [13]. PtEst1 tolerated up to 10% (v/v) acetonitrile and 30% (v/v) methanol, showing a slow decrease in esterase activity to 35% and 98% residual activity after 96-h incubation in the presence of acetonitrile and methanol, respectively (Fig. 2C,D).

**Table 1.**  $k_{\text{cat}}$  ( $\text{min}^{-1}$ ) of PtEst1 measured for 62 structurally different carboxylic esters found to be hydrolyzed out of 96 tested. For activity determination (in triplicates, with standard deviation shown), calculated on a continuous pH indicator assay, conditions are as follows: [enzyme], 45  $\mu\text{g}\cdot\text{mL}^{-1}$ ; [ester], 10  $\text{mg}\cdot\text{mL}^{-1}$  to ensure saturating concentrations; reaction volume, 44  $\mu\text{L}$ ;  $T$ , 30 °C; pH, 8.0. Absence of activity was defined as at least two-fold background signal. For  $k_{\text{cat}}$  calculations, SIGMA PLOT 14.0 (Systat Software GmbH, Erkrath, Germany) was used. Under our assay conditions, no activity was detected toward: glyceryl trioctanoate, triolein, dodecanoil acetate, pentadecyl acetate, ethyl acetate, ethyl decanoate, ethyl dodecanoate, ethyl myristate, (1R)-(–)-menthyl acetate, (1S)-(+)-menthyl acetate, *n*-benzyl-L-proline ethyl ester, *n*-benzyl-D-proline ethyl ester, methyl 3-hydroxybenzoate methyl 2-hydroxybenzoate, benzylparaben, methyl decanoate, methyl oleate, methyl dodecanoate, methyl myristate, phenylethyl cinnamate, methyl 2,5-dihydroxycinnamate, methyl cinnamate, methyl ferulate, vinyl laurate, vinyl myristate, vinyl palmitate, vinyl oleate, D-pantolactone, L-pantolactone, (1R)-(–)-dimethyl succinate, 2,4-dichlorophenyl 2,4-dichlorobenzoate, 2,4-dichlorobenzyl 2,4-dichlorobenzoate, diethyl-2,6-dimethyl 4-phenyl-1,4-dihydro pyridine-3,5-dicarboxylate, glyceryl trilaurate.

Ester library	$k_{\text{cat}}$ ( $\text{min}^{-1}$ )
Ethyl 3-oxohexanoate	3574.5 $\pm$ 17.1
Ethyl propionylacetate	3513.5 $\pm$ 14.4
Ethyl acetoacetate	2016.7 $\pm$ 15.5
Vinyl propionate	3924.7 $\pm$ 17.3
Vinyl butyrate	3463.5 $\pm$ 20.5
Ethyl butyrate	2464.9 $\pm$ 17.8
Phenyl propionate	1762.6 $\pm$ 12.1
Phenyl acetate	1757.5 $\pm$ 13.8
Ethyl ( <i>R</i> )-(+)-4-chloro-3-hydroxybutyrate	1726.8 $\pm$ 19.6
Vinyl benzoate	1708.4 $\pm$ 18.4
Glyceryl tripropionate	1689.2 $\pm$ 15.1
Ethyl 2-ethylacetoacetate	1675.1 $\pm$ 13.5
Glyceryl tributyrate	1664.6 $\pm$ 21.9
Glyceryl triacetate	1663.2 $\pm$ 16.7
Ethyl 2-methylacetoacetate	1632.4 $\pm$ 18.7
(–)-Ethyl L-lactate	1605.3 $\pm$ 19.6
Ethyl benzoate	1563.4 $\pm$ 16.8
Vinyl crotonate	1544.6 $\pm$ 19.8
Methyl ( <i>R</i> )-(–)-mandelate	1538.8 $\pm$ 20.9
Propyl acetate	1536.2 $\pm$ 15.0
(+)-Ethyl D-Lactate	1519.6 $\pm$ 15.1
3-Methyl-3-buten-1-yl acetate	1501.9 $\pm$ 19.7
1-Naphthyl acetate	1490.7 $\pm$ 15.2
Ethyl ( <i>S</i> )-(–)-4-chloro-3-hydroxybutyrate	1471.5 $\pm$ 13.9
Hexyl acetate	1458.9 $\pm$ 15.5
Methyl ( <i>S</i> )-(+)-mandelate	1448.8 $\pm$ 13.1
Ethyl hexanoate	1408.6 $\pm$ 15.4
Ethyl 2-chlorobenzoate	1382.6 $\pm$ 17.9
Propyl hexanoate	1272.7 $\pm$ 14.5
(+)-Methyl D-Lactate	1172.5 $\pm$ 13.0
Butyl acetate	1123.4 $\pm$ 15.8
Propyl butyrate	1061.2 $\pm$ 26.0
Benzyl ( <i>R</i> )-(+)-2-hydroxy-3-phenylpropionate	1025.0 $\pm$ 12.7
Vinyl acrylate	1005.1 $\pm$ 16.0

**Table 1.** (Continued).

Ester library	$k_{\text{cat}}$ ( $\text{min}^{-1}$ )
Propyl propionate	950.2 $\pm$ 11.1
Methyl butyrate	912.2 $\pm$ 18.5
Cyclohexyl butyrate	829.8 $\pm$ 10.3
Ethyl propionate	824.0 $\pm$ 15.2
Methyl glycolate	795.1 $\pm$ 15.0
Methyl hexanoate	787.8 $\pm$ 12.9
Octyl acetate	762.2 $\pm$ 25.4
Vinyl acetate	689.8 $\pm$ 18.7
(+)-Methyl (S)-3-hydroxyvalerate	455.2 $\pm$ 12.7
(-)-Methyl L-Lactate	424.8 $\pm$ 11.2
Phthalic acid diethyl ester	420.8 $\pm$ 12.7
Methyl benzoate	419.8 $\pm$ 14.1
Geranyl acetate	376.8 $\pm$ 8.8
(-)-Methyl (R)-3-hydroxyvalerate	341.3 $\pm$ 13.4
$\gamma$ -Valerolactone	340.2 $\pm$ 11.6
Isobutyl cinnamate	130.2 $\pm$ 4.6
Methyl octanoate	114.6 $\pm$ 10.7
n-Pentyl benzoate	84.6 $\pm$ 1.2
1-Naphthyl butyrate	84.0 $\pm$ 1.9
Glucose pentaacetate	82.9 $\pm$ 3.7
Butylparaben	73.4 $\pm$ 2.0
Ethyl octanoate	68.1 $\pm$ 1.5
Propylparaben	63.4 $\pm$ 1.8
Benzoic acid, 4-formyl-phenylmethyl ester	62.1 $\pm$ 1.7
(1S)-(+)-Neomenthyl acetate	49.4 $\pm$ 1.9
(+)-Methyl (S)-3-hydroxybutyrate	36.0 $\pm$ 1.6
(1R)-(+)-Neomenthyl acetate	27.5 $\pm$ 1.6
(-)-Methyl (R)-3-hydroxybutyrate	8.6 $\pm$ 0.4

Higher concentrations of both methanol and acetonitrile led to a fast decrease of enzyme activity.

Unexpectedly, the absence of organic solvent caused a rapid decrease of activity too, whereas low concentrations of acetonitrile and methanol induced a stabilization of the enzyme, shown by only minor decline in enzymatic activity. However, the stabilization effect could not be linked to a stabilization of the protein structure level as indicated by thermal melting point ( $T_{m50}$ ) measurements using nano differential scanning fluorimetry (Fig. 2E,F). In contrast to the measurement of residual enzyme activity after incubation in organic solvent, the thermal stability of the protein structure of PtEst1 is reduced with increasing concentration of methanol and acetonitrile.

For structural studies of the enzyme, methyl 4-methylumbelliferyl hexylphosphonate (M4MHP) was chosen as covalently binding substrate analogue for co-crystallization. In accord with the results of the substrate profiling, this ester that consists of an aromatic alcohol unit and a short alkyl chain proved to be converted efficiently and consequently inhibited the enzyme effectively. In comparison with PMFS, which

inhibited the protein activity resulting in a residual activity of 80–95%, the M4MHP inhibitor completely inhibited the PtEst1 protein in solution (Fig. 3). M4MHP is a common suicide inhibitor for lipases, which was used for active site titration in CalB, for example [14]; the phosphonate ester is hydrolyzed by the enzyme, producing free 4-methylumbelliferone, and the hexyl(methoxy)phosphinic acid, however, forms a stable tetrahedral adduct, covalently attached to the enzyme's catalytic serine, as it is known for other serine hydrolases [15].

### Overall structure of PtEst1

We set out to crystallize the PtEst1 protein to determine its structure in the apo as well as inhibitor-bound state experimentally. Well-diffracting crystals were obtained as described in the [Materials and methods](#) section. For the apo PtEst1 structure, a dataset was collected and the structure was refined up to a resolution of 1.35 Å ( $R_{\text{work}}$  and  $R_{\text{free}}$  values were 13.7% and 18.4%, respectively). The PtEst1 structure in complex with the hexyl(methoxy)phosphinic acid (HPA) part of the inhibitor methyl 4-methylumbelliferyl hexylphosphonate (M4MHP) covalently bound at the active site Ser202 mimics the transition state of the catalytic cycle. Well-diffracting crystals of the inhibitor complex allowed data collection and structure refinement up to a resolution of 1.81 Å ( $R_{\text{work}}$  and  $R_{\text{free}}$  values were 15.1% and 19.2%, respectively). All data statistics are given in Table 2.

Both protein crystal structures displayed two monomers in the asymmetric unit, which by close inspection appears to be a crystallization dimer.

The PtEst1 protein consists of 368 residues and exhibits a canonical  $\alpha\beta$ -hydrolase fold with the typical catalytic triad composed of Ser, His, Asp (Ser202 as the nucleophile, His338 as the proton acceptor/donor, and Asp308 as the residue stabilizing the His in PtEst1).

Similar to other esterases described so far, PtEst1 is likewise composed of two domains: the catalytic domain (residues 81–368) and the cap domain (residues 12–80) (Fig. 4). The catalytic domain is composed of a twisted, central eight-stranded  $\beta$ -sheet, which is predominantly parallel with only  $\beta$ -strand 2 being in anti-parallel orientation (strand order  $\beta$ 1,  $\beta$ 2,  $\beta$ 4,  $\beta$ 3,  $\beta$ 5,  $\beta$ 6,  $\beta$ 7, and  $\beta$ 8). It is surrounded by eight helices, two in the concave side of the sheet ( $\alpha$ 3 and  $\alpha$ 10), and six along the convex side ( $\alpha$ 4,  $\alpha$ 5,  $\alpha$ 6,  $\alpha$ 7,  $\alpha$ 8, and  $\alpha$ 9). Between helix  $\alpha$ 8 and  $\beta$ -strand 7 two short helical elements are present ( $\eta$ 2 and  $\eta$ 3). The cap domain is formed by the N-terminal sequence region (residues 12–80) that mainly contains helical structure

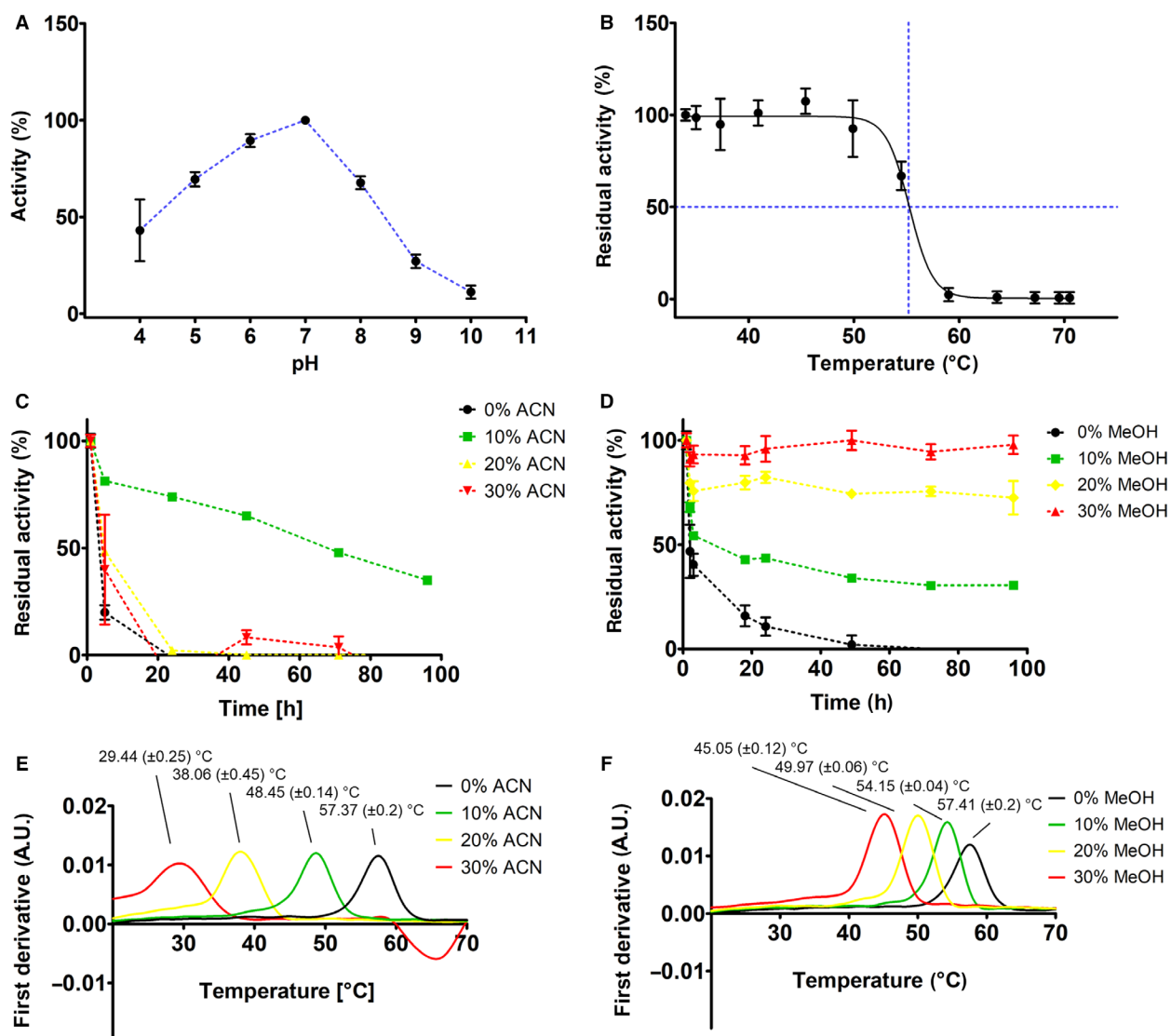


**Fig. 2.** Biochemical properties of PtEst1. (A) pH optimum for esterase activity determined via *p*NPB hydrolysis in Britton-Robinson buffer with different pH values. (B) Melting curve of PtEst1 determined by incubation of protein solution for 1 h at the respective temperature and subsequent determination of residual activity in relation to the lowest temperature (34 °C). Data points were fitted (black line) using GRAPH PAD PRISM software with the Boltzmann sigmoidal equation. (C) Residual activity of PtEst1 after incubation with 0% (black), 10% (green), 20% (yellow), or 30% (red) acetonitrile (ACN) or (D) methanol for 96 h. The activity is shown relative to T0 for the respective organic solvent concentration. (E) First derivative of thermal melting curves measured as the ratio 350/330 nm by nano differential scanning fluorimetry (nanoDSF) of PtEst1 with 0–30% acetonitrile or (F) 0–30% methanol; the melting temperature (T<sub>m50</sub>) is given above each curve. Mean and standard deviation of three reactions are shown; the color code is the same as in (C) and (D). Each measurement was repeated at least three times ( $n = 3$ ), and the error bars represent the standard deviation.

elements (helices  $\alpha 1$  and  $\alpha 2$ , led by a short helical structure  $\eta 1$ ) and their connecting loops. This cap domain flanks the carboxy-edge of the central  $\beta$ -sheet, particularly strands  $\beta 4$ ,  $\beta 3$ ,  $\beta 5$ ,  $\beta 6$ ,  $\beta 7$ , and  $\beta 8$  (Fig. 4).

A search for structural homologues of PtEst1 using the Dali protein structure comparison server (<http://ekhidna2.biocenter.helsinki.fi/dali/>) identified the

closest homologues as esterase mutant F72G (pdb-code: 5IQ0, to be published), the esterase CinB from *Enterobacter asburiae* (pdb-code: 6KMO [16]), the fungal esterase EstA from *Rhizomucor miehei* (pdb-code: 4WY5 [17]), and the acetyl esterase Aes from *E. coli* (pdb-code: 4KRY [18]). The unpublished esterase mutant F72G had the highest Z-score with 58.0 and a



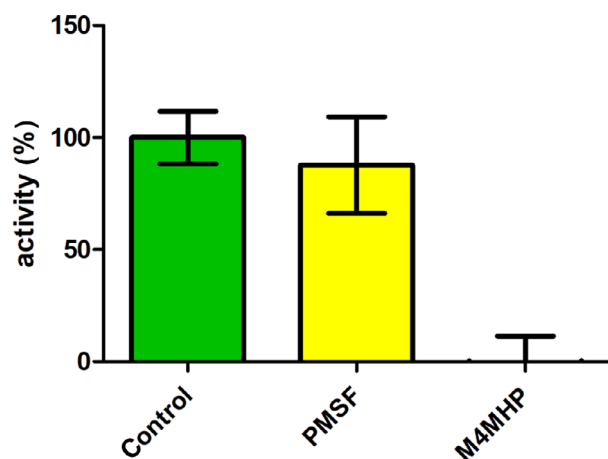


**Fig. 3.** Inhibitor study with PtEst1. 100 nM PtEst1 was combined with 1 mM of phenylmethylsulfonyl fluoride (PMSF), methyl 4-methylumbelliferyl hexylphosphonate (M4MHP), or water (control) in 100 mM potassium phosphate buffer pH 7.4 for 1 h at room temperature, before the enzyme activity was determined with pNPB as a substrate. The control reaction was set as 100% activity. Mean and standard deviation of three reactions are shown. Each measurement was repeated at least three times ( $n = 3$ ), and the error bars represent the standard deviation.

root-mean-square deviation (rmsd) of 1.1 Å over 351 Cα atoms along with a high sequence identity of 56%. The corresponding values for the ten closest homologues of PtEst1 are given in Table 3. The overall fold within these 10 structures is highly similar with most of the proteins being classified as esterases, although their sequence identity is rather low (14–27%). The highest rmsd is 3.1 Å for a probable gibberellin receptor from *Arabidopsis thaliana*.

### Active site

The active site of PtEst1 is identified by the highly conserved residues of the catalytic triad consisting of Ser202, His338, and Asp308 (Fig. 5). The catalytic Ser202 is part of the conserved sequence motif GX SXG within the nucleophilic elbow, which is a sharp turn connecting β5 and α5 (in PtEst1: Gly200, Glu201, Ser202, Gly203, Gly204). The typical ‘oxanion hole’ of a GGGX type which stabilizes the tetrahedral intermediate in ester hydrolysis is composed of Gly127 and Gly128 within the sequence motif HGGG [5] (residues 125–128 in PtEst1) at a distance of around 4.5 Å to Ser202 (Fig. 5). The Ser202 Oγ atom is in hydrogen bonding distance to the Ne2 atom of His338 (2.7 Å), which is in turn hydrogen bonded with its Nδ1 to Oδ1 and Oδ2 of Asp308 (3.2 and 2.7 Å).

**Table 2.** Data collection and refinement statistics of PtEst1 in apo- and inhibitor-bound form.

	PtEst1 apo	PtEst1 inhibitor
<b>Data collection</b>		
Beamline	DESY, P14	ESRF, ID29
Wavelength [Å]	0.9762	0.9762
Resolution range [Å]	55.22–1.353 (1.402–1.353)	43.39–1.811 (1.875–1.811)
Space group	P 21 2 21	P 21 21 21
Unit cell [Å, °]	58.71 77.19 162.51 90 90 90	72.41 86.7 110.11 90 90 90
Total reflections	964948 (31201)	312917 (31685)
Unique reflections	155980 (10966)	63348 (6223)
Multiplicity	6.2 (2.8)	4.9 (5.1)
Completeness (%)	96.69 (68.71)	98.93 (99.28)
Mean I/σ(I)	16.64 (1.84)	10.30 (2.31)
Wilson B-factor [Å <sup>2</sup> ]	14.00	15.69
R-merge	0.05706 (0.488)	0.1042 (0.5546)
R-meas	0.06212 (0.5718)	0.1165 (0.6186)
R-pim	0.02426 (0.2885)	0.05104 (0.2696)
CC1/2	0.999 (0.804)	0.996 (0.82)
CC*	1 (0.944)	0.999 (0.949)
<b>Refinement</b>		
Refinement [Å]	55.28–1.353 (1.388–1.353)	43.39–1.811 (1.858–1.811)
Reflections used in refinement	153608 (6671)	59945 (4430)
Reflections used for R-free	1994 (88)	3152 (200)
R-work	0.137 (0.300)	0.151 (0.227)
R-free	0.184 (0.328)	0.192 (0.262)
Number of nonhydrogen atoms	6484	6482
Macromolecules	5507	5462
Ligands	41	58
Solvent	936	962
Protein residues	720	721
RMS (bonds)	0.005	0.010
RMS (angles)	1.617	1.648
Ramachandran favored (%)	97.44	96.39
Ramachandran allowed (%)	2.56	3.51
Ramachandran outliers (%)	0	0.1
Average B-factor [Å <sup>2</sup> ]	18.01	17.0
PDB-code	6Z68	6Z69

Both the catalytic triad and the oxanion hole are located in a deep tunnel as it is characteristic for many αβ-hydrolase fold proteins. In the apo structure of PtEst1, the entrance of that tunnel is closed through mainly hydrophobic side chains (Phe259, Ile260 from the loop connecting α7 and α8, and Phe72 and Leu264

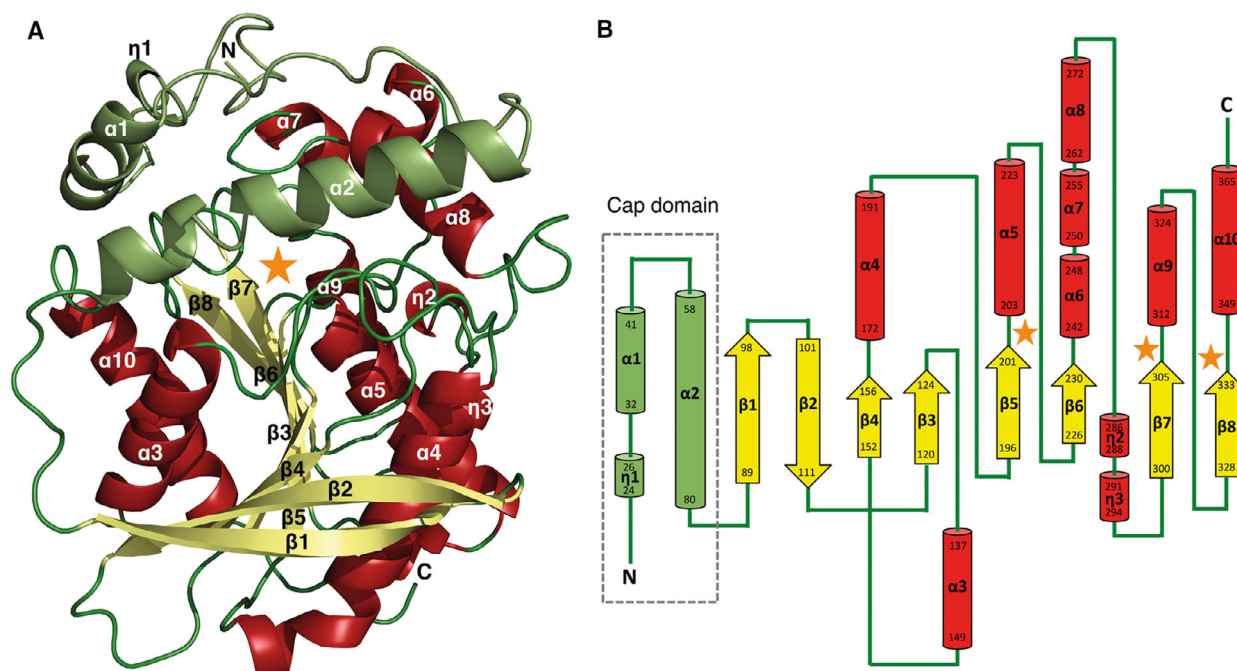


**Fig. 4.** Overall structure of the metagenomic family IV esterase PtEst1. (A) Cartoon representation of one PtEst1 monomer (pdb-code 6Z68) with the position of the catalytic triad highlighted with an orange star. The cap domain is highlighted in green. (B) Topology diagram of PtEst1 esterase with the position of the catalytic residues marked with orange stars and the cap domain surrounded by the dashed line;  $\alpha$ -helices are shown as cylinders and  $\beta$ -strands as arrows. Figure showing the structure was generated using PYMOL 2.4.0 ([www.pymol.org](http://www.pymol.org)).

from helices  $\alpha 2$  and  $\alpha 8$ , respectively). In contrary, this active site is opened and widened in the inhibitor-bound complex (Fig. 6), which is achieved by some minor conformational changes, as is also reflected by the very low rmsd value of 0.5 Å over 289 C $\alpha$  atoms: Phe259 and Ile260 show identical positions and orientations compared to the apo form, whereas the side chain of Leu264 is rotated outwards (about 3.4 Å). The middle part of helix  $\alpha 2$  (part of the cap domain) is minorly bended outwards (about 1 Å), and together with a different side chain conformation of Phe72, the entrance is widened by around 2.5 Å (Fig. 7). This opening of the tunnel in the inhibitor-bound structure results in a larger volume of the active site by almost 50%: The volume of the active site is 988 Å<sup>3</sup> and of the inhibitor-bound state 1416 Å<sup>3</sup>.

Interestingly, in the apo PtEst1 crystal structure the active site is occupied by a ligand, as became obvious when looking at the electron density, which was identified as PEG molecule arising from the crystallization solution (Fig. 5A). This PEG molecule is clearly visible in the electron density and is coordinated by interaction with Ser202 and the backbone nitrogen of Gly127, and both residues are part of the active site as described above. Additionally, the PEG molecule is

coordinated by a water molecule. At the same position in the inhibitor-bound PtEst1 structure, at the bottom of the funnel HPA is covalently bound to Ser202, further coordinated by the cleaved off 4-methylumbelliferone (MUB), which is still present in the tunnel (Fig. 5B). This is unusual and likely in solution MUB diffuses out of the active site. MUB is trapped in the crystals due to an extra M4MHP molecule, which was found at the outer entrance of the catalytic funnel (Fig. 6B,D).

HPA is covalently bound to Ser202 and is held in place by hydrogen bonds to several backbone N atoms via its phosphate O3P atom to the N atom of Gly203, Gly127, and Gly128 (all 2.8 Å), whereas the latter are part of the oxyanion hole. Via the phosphate O2P atom, the analogue HPA is weakly hydrogen bonded to the O05 atom (3.5 Å) of the split off MUB. In turn, MUB interacts with its O13 atom to the backbone nitrogen atom of Ser261 and a water molecule (Fig. 5). The additionally present M4MHP molecule at the entrance of the active site funnel is positioned only by nonpolar interactions with the mainly hydrophobic surface residues. The inhibitor is also coordinated by three water molecules. In the apo structure, the position of the extra M4HMP molecule, the hydrophobic

**Table 3.** Structure-based alignment of apo-PtEst1 against pdb entries. Top 10 of the most similar structures are given with their corresponding alignment quality (Z-score), root mean square deviation (RMSD), number of aligned residues ( $N_{\text{align}}$ ), their sequence identity (Seq-%), their PDB number (Target PDB), and description of the PDB entry (Protein).

Apo-PtEst1 (pdb-code: 6Z68)						
##	Z-score	RMSD	$N_{\text{align}}$	Seq-%	Target PDB	Protein
1	58.0	1.1	351	56	5IQ0:A	Esterase mutant ( <i>uncultured bacterium</i> )
2	38.5	2.2	304	26	6KMO:A	Esterase CinB ( <i>Enterobacter asburiae</i> )
3	35.9	2.4	304	27	4WY5:A	Esterase EstA ( <i>Rhizomucor miehei</i> )
4	35.4	2.4	302	16	4KRY:E	Esterase Aes ( <i>Escherichia coli</i> )
5	32.1	2.3	292	20	4C87:A	Esterase Est1 ( <i>Lactobacillus plantarum</i> WCFS1)
6	32.1	2.7	302	19	4Q05:A	Esterase E25 ( <i>uncultured bacterium</i> )
7	31.6	3.1	296	25	2ZSI:A	Probable gibberellin receptor GID1 ( <i>Arabidopsis thaliana</i> )
8	30.7	2.8	285	17	4N5H:X	Esterase B ( <i>Lactobacillus rhamnosus</i> Lc 705)
9	29.8	2.8	278	14	3D7R:A	Putative esterase ( <i>Staphylococcus aureus</i> sp. aureus)
10	29.7	2.6	271	20	2O7R:A	Carboxylesterase CXE1 ( <i>Actinidia eriantha</i> )

patch of helix  $\alpha 2$ , was occupied by PEG and is also containing residual electron density, which might be another PEG molecule as well. Since helix  $\alpha 2$  is part of the CAP domain, which is important for activity, it appears to be an initial docking point for the substrate prior to entering the tunnel and thereby the active site of PtEst1.

## Discussion

The metagenomic esterase PtEst1 identified in this study most probably originates from a bacterium

belonging to the genus *Pseudonocardia*. In line with the results of this study, these bacteria are frequently found in wastewater treatment plants as being capable of the degradation of cyclic molecules like cyclohexanone or dioxane [19]. Besides moderate thermostability and organic solvent tolerance, the biochemical characterization of the enzyme revealed a considerable substrate promiscuity, which appears to be a common feature of family IV esterases [10]. In relation to the results from this previous study, this enzyme belongs to the 10% most promiscuous enzymes, comparable to the well-known and frequently used lipase CalB from *Pseudozyma aphidis* (formerly *Candida antarctica*). The analysis of the substrate specificity revealed that PtEst1 was able to hydrolyze a broad variety of esters, such as paraben esters (i.e., propyl and butyl paraben), lactones (i.e.,  $\gamma$ -valerolactone), ester derivatives of cinnamic acid (i.e., isobutyl cinnamate), and chiral esters such as neomenthyl acetate. These activities, together with the remarkable preference of this enzyme for oxo esters (i.e., ethyl 3-oxohexanoate being the preferred substrate) compared to other similar enzymes [10], highlight novel features displayed by PtEst1.

The moderate tolerance of PtEst1 for organic solvents resulted in an increased residual activity after incubation of the enzyme in the presence of low amounts of acetonitrile or methanol compared to samples without organic solvent. Incubation of PtEst1 in the presence of organic solvents, however, did not result in an enhanced thermal stability. Thus, the stabilization effects might be temperature dependent, for example, caused by preventing protein aggregation in the assay buffer. Such effects have been previously described for organic solvents and are for example used for the solubilization of proteins, which aggregate as inclusion bodies during strong recombinant expression [20].

Substrate promiscuity of esterases was predicted as dependent on the ratio of cavity volume and solvent accessible surface area within the active site [10]. The crystal structure of PtEst1 confirms that. The protein contains an N-terminal cap domain, which is rather common for GGGX type  $\alpha/\beta$  hydrolases, leaving a narrow tunnel to the active site allowing for substrate entry [5]. As a result of conformational changes of the cap domain, the active site cavity of the inhibitor bound, and the apo structure differ in their volume. The apo structure shows an active site cavity volume of 988 Å<sup>3</sup>, the inhibitor-bound structure of 1416 Å<sup>3</sup>. This flexibility might contribute to the prominent substrate promiscuity observed for PtEst1. The unique situation of a remaining MUB molecule in the active site illustrates the size of the active site cavity, shielded



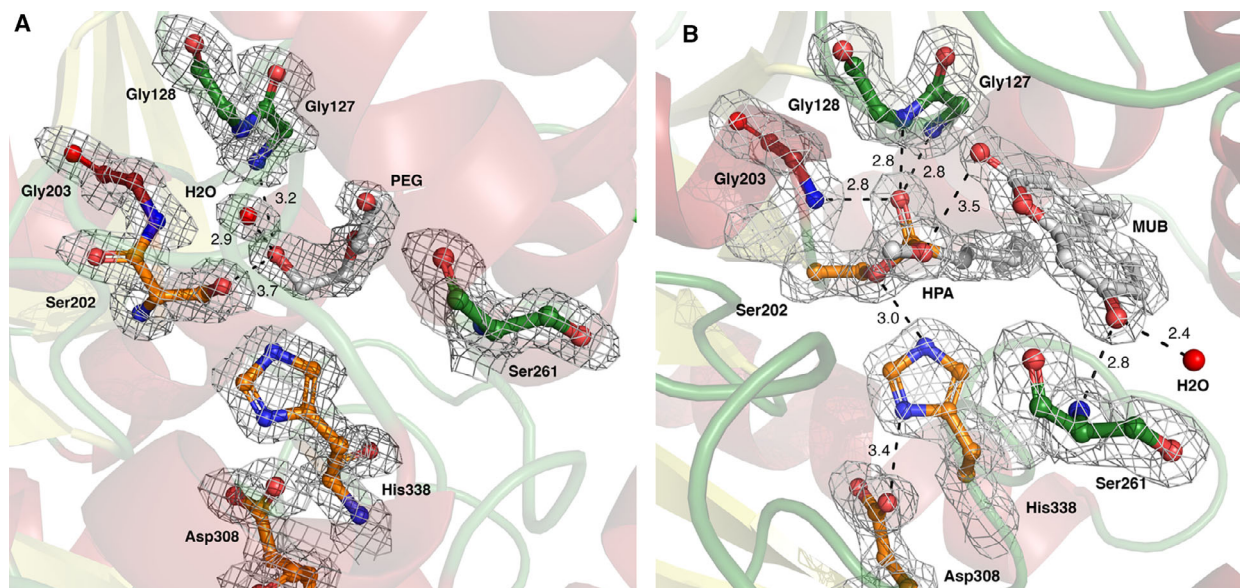


**Fig. 5.** Architecture of the catalytic site in apo (A; pdb-code 6Z68) and inhibitor-bound PtEst1 (B; pdb-code 6Z69). The catalytic triad is composed of Ser202, His338, and Asp308 (shown as orange sticks). In the apo structure, a PEG molecule is bound in the active site (A). In the inhibitor complex, hexyl(methoxy)phosphinic acid (HPA) is covalently bound to Ser202. In close proximity, the cleaved 4-methylumbelliferone molecule (MUB) is clearly visible in the electron density (B). Gly203 is the first aa of the adjacent helix  $\alpha 5$ , Ser261 is located in the loop connecting  $\alpha 7$  and  $\alpha 8$ . Gly127 and Gly128 are part of the HGGG motif and create the oxyanion hole. Distances between selected atoms are given in Å, and densities are contoured at 1  $\sigma$ . Figures showing structures were generated using PYMOL 2.4.0.

from the solvent by a cap domain, leaving a funnel like entrance to the catalytic gorge. Interestingly, MUB was only present in the active site when a M4MHP molecule was located at a hydrophobic patch of helix  $\alpha 2$  at the same time, probably blocking the funnel exit. In the apo structure, in absence of M4MHP molecules, the hydrophobic patch of helix  $\alpha 2$  was occupied by PEG, suggesting a specific function in substrate binding for PtEst1. Lipase/esterase structures with substrates in different states are only rarely available. Nonetheless, a similar situation can be found, interestingly, in structures of Est22 recovered from a Deep-Sea metagenome. This likewise family IV/GGGX type esterase was co-crystallized with *p*-nitrophenol leaving groups of an esterase substrate. One structure includes a *p*-nitrophenol attached to a hydrophobic patch at the cap domain, which apparently binds another molecule of *p*-nitrophenol within the active site cavity. Although the localization of the patch is different from the situation in PtEst1, this suggests a substrate prerecognition mechanism by hydrophobic patches of the cap domains. It might be speculated if such a rather unspecific substrate pre-binding mechanism might contribute to the substrate promiscuity that was frequently observed for this esterase family.

To conclude, PtEst1 may be considered a solvent-resistant and moderately thermostable hydrolase with prominent substrate ambiguity without enantioselectivity. While the applicability of this enzyme with high substrate ambiguity, further structure-based screening of specificity/selectivity determinants and engineering efforts will help to determine to what extent this enzyme can be engineered to introduce chiral specificity while maintaining prominent substrate ambiguity, an uncommon feature among enzymes.

## Materials and methods

### Library construction

Five environmental samples from a wastewater treatment plant were used as inoculum (500  $\mu$ L) for enrichment cultures in 50 mL M9 minimal medium [M9 Minimal Salts (Sigma-Aldrich, Taufkirchen, Germany) (5  $\times$  stock solution); Mg-solution 20 g·L<sup>-1</sup> MgSO<sub>4</sub>  $\times$  7 H<sub>2</sub>O; Ca-solution 2 g·L<sup>-1</sup> CaCl<sub>2</sub>  $\times$  2 H<sub>2</sub>O; trace element solution 1.6 g·L<sup>-1</sup> MnSO<sub>4</sub>; 2.8 g·L<sup>-1</sup> H<sub>3</sub>BO<sub>3</sub>; 0.04 g·L<sup>-1</sup> Cu(NO<sub>3</sub>)<sub>2</sub>; 0.24 g·L<sup>-1</sup> ZnSO<sub>4</sub>; 0.8 g·L<sup>-1</sup> Na<sub>2</sub>MoO<sub>4</sub>; iron solution 5 g·L<sup>-1</sup> FeSO<sub>4</sub>; 0.16% (v/v) HCl mixed in a ratio of 20%, 1%, 1%, 0.1%, 0.12%, 77.78% sterile VE water] and 10 g·L<sup>-1</sup> cyclohexanol succinate as an esterase substrate

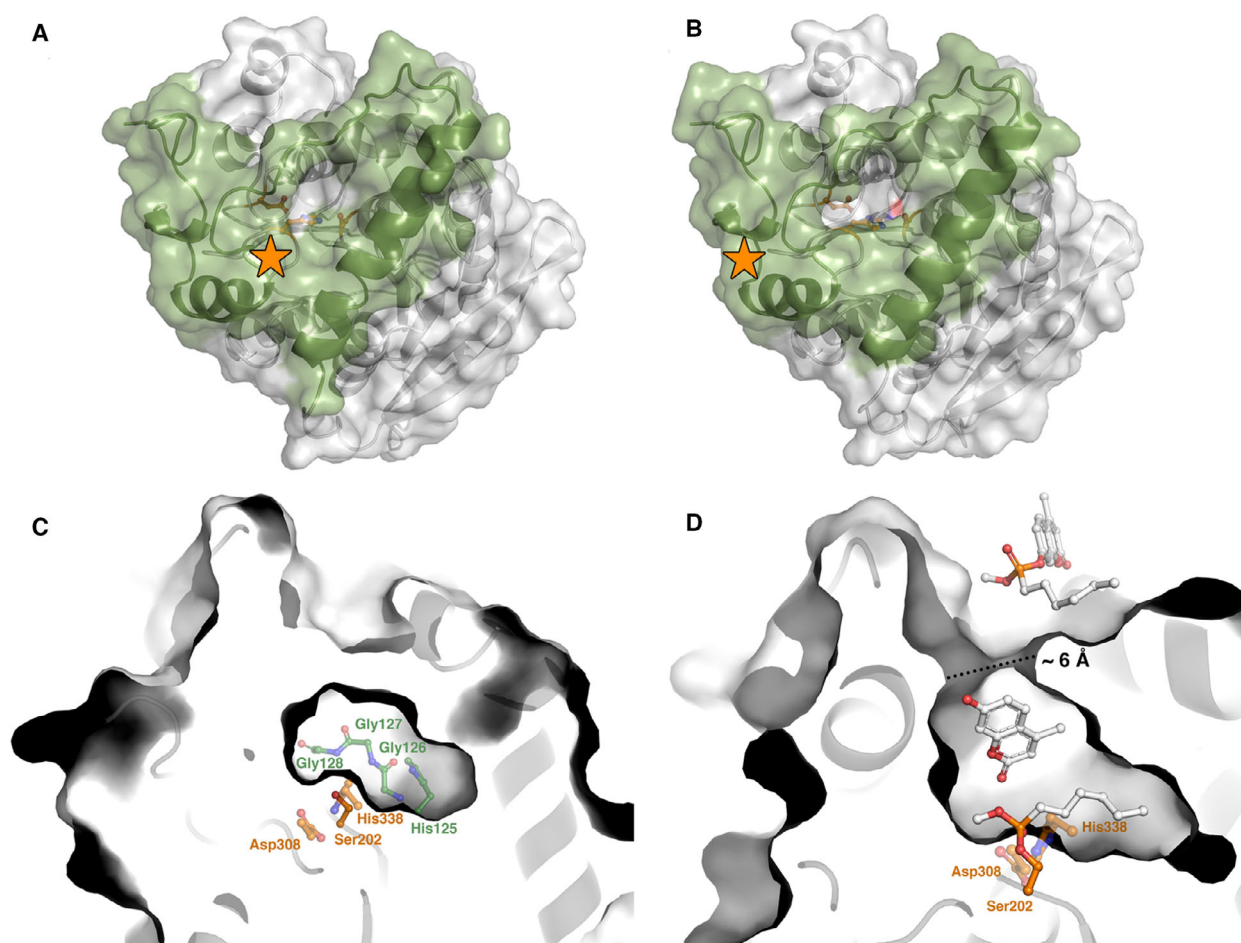


**Fig. 6.** Surface representation of PtEst1 esterase in apo (A; pdb-code 6Z68) and inhibitor-bound state (B; pdb-code 6Z69), illustrating the cap domain (green) and the funnel-shaped catalytic gorge. Residues of the catalytic triad buried inside the catalytic tunnel are shown as orange sticks, inhibitor M4MHP as gray sticks. Main differences of the tunnel accessibility are located on top of the orange stars. Cross section through the surface of PtEst1 to show the catalytic gorge in the apo protein (C) and with bound ligands (D), shown as white sticks. (C): On the bottom of the catalytic tunnel, the four residues of the HGGG motif, forming the oxyanion hole, are highlighted as green sticks. Residues of the catalytic triad are Ser202, His338, and Asp308 (all in orange sticks; Asp and His are faded for clarity although they were in the foreground). In the apo structure, the entrance of the catalytic tunnel is closed. (D) Deep inside the funnel the hexyl(methoxy)phosphonic acid part of the inhibitor methyl 4-methylumbelliferyl hexylphosphonate is covalently bound to the catalytic Ser. Above the covalently bound hexyl(methoxy)phosphonic acid, the cleaved 4-methylumbelliferone is present. Here, the active site tunnel is open with a diameter of around 6 Å in the narrowest part (dashed line). At the entrance of the active site funnel, an additional molecule methyl 4-methylumbelliferyl hexylphosphonate is present. Figures showing structures were generated using PYMOL 2.4.0.

were supplemented as sole carbon source at 50 °C. After 6 weeks of incubation, 1 mL of the enrichment culture was used to inoculate a new enrichment culture at the same conditions. The procedure was repeated for a third time, and 40 µg·mL<sup>-1</sup> cycloheximide was added to the enrichment culture to select for prokaryotes. After three rounds of enrichment, the cells were harvested by centrifugation (30 min, 3220xg) and metagenomic DNA was extracted by chemical lysis and phenol-chloroform extraction as described earlier [21]. The metagenomic DNA library was constructed using the TOPO XL PCR Cloning Kit

(Invitrogen, Life Technologies, Darmstadt, Germany) as described for genomic libraries before [22].

### Screening

The metagenomic library was screened using *E. coli* TOP10 as a host and tributyrin containing agar plates for the identification of esterase producing clones as described earlier [23]. Clones exhibiting a clearing halo were collected, and their esterase activity was verified with 4-nitrophenyl butyrate (pNPB) as a substrate, as described before [24]. To determine

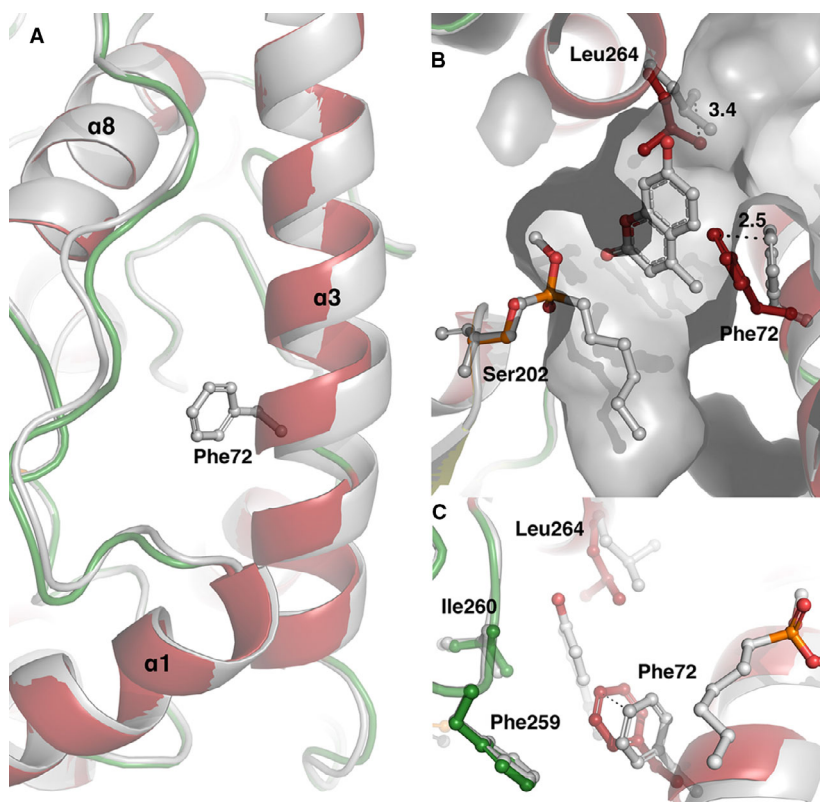


**Fig. 7.** Opening of the active site tunnel in PtEst1. Apo structure is shown in red/green (pdb-code 6Z68), inhibitor complex in gray (pdb-code 6Z69). (A) An overview of the adjacent secondary elements is given. In the complex structure helix  $\alpha 2$  is slightly bended outwards. (B) Cross section through the catalytic tunnel. Cleaved inhibitor molecules hexyl(methoxy)phosphinic acid (HPA) and 4-methylumbelliferone molecule (MUB) are deep inside the tunnel with HPA covalently bound to Ser202, and MUB close to Phe72 and Leu264. By comparing the apo with the complex structure, mainly the side chains of Phe72 and Leu264 differ after substrate/product binding, thus creating more space in the catalytic tunnel (3.4 and 2.5 Å, respectively). Phe259 and Ile260 adopt a very similar position in both structures and therefore do not play a role in widening the funnel (C). Figures showing structures were generated using Pymol 2.4.0.

the enzyme coding gene, plasmid DNA was extracted from cell culture of active clones with the innuPREP Plasmid Mini Kit 2.0 (Analytik Jena, Jena, Germany). The terminal ends of the insert DNA were sequenced (MWG Eurofins Genomics, Ebersberg, Germany) using the oligonucleotides included in the TOPO XL PCR Cloning Kit (Invitrogen). The resulting fragments were used to perform a search for open reading frames with ORF finder [25].

### Cloning, expression and purification

The gene coding for the enzyme PtEst1 (GenBank Accession No. MT942606) was cloned into expression vector pET-22b(+) (Novagen, Merck, Darmstadt, Germany) in frame with the vector encoded hexahistidine-tag utilizing *Nde*I and *Xho*I endonuclease restriction sites [26]. The gene was amplified by polymerase chain reaction (PCR) using the plasmid DNA from the library clone Cyc\_TB#025 as a template. Phusion High-Fidelity DNA Polymerase (Thermo Scientific, Waltham, MA, USA) was used following the manufacturer's recommendations, with the oligonucleotides Cyc-TB-025\_fw (5'→3': GCGCATATGACGACGACGTC GAACTC) and Cyc-TB-025\_rv22b (5'→3': GCTCTCGA GGCGGTGCAGGCTCGTG). The resulting recombinant plasmid pET22b\_PtEst1 was used to transform chemical competent *E. coli* DH5 $\alpha$  cells [27] for replication. The DNA sequence of the cloned gene was sequenced using T7

and T7 term standard primers (LGC Genomics, Berlin, Germany).

Protein production was carried out in Erlenmeyer flasks filled to 1/10 of the maximal volume with auto induction media as described in ([https://openwetware.org/wiki/Lidstrom:Autoinduction\\_Media](https://openwetware.org/wiki/Lidstrom:Autoinduction_Media)) supplemented with 100  $\mu\text{g}\cdot\text{mL}^{-1}$  ampicillin, for 9 h at 25 °C with shaking (160 r.p.m.). The culture was inoculated to an optical density of 0.05 ( $\lambda = 580 \text{ nm}$ ) from a culture of *E. coli* LOBSTR grown overnight in LB media (Luria/Miller, Carl Roth GmbH & Co. KG, Karlsruhe, Germany) supplemented with 0.5% glucose and 100  $\mu\text{g}\cdot\text{mL}^{-1}$  ampicillin. After 9 h, cells were collected by centrifugation for 30 min at 6000 g, 4 °C, the supernatant was discarded, and cell pellets were stored at −20 °C or used subsequently.

Purification of PtEst1 was performed by immobilized metal ion affinity chromatography (IMAC) followed by size exclusion chromatography (SEC) as described earlier [28], with minor modifications. The lysis buffer for IMAC was used without addition of imidazole (20 mM  $\text{Na}_2\text{HPO}_4$  pH 7.4, 500 mM NaCl), and the washing buffer was supplied with 10 mM imidazole (20 mM  $\text{Na}_2\text{HPO}_4$  pH 7.4, 500 mM NaCl, 10 mM imidazole). For SEC, the mobile phase was composed of 100 mM potassium phosphate buffer pH 7.4.

Protein concentrations were determined using a micro-volume spectrophotometer (NanoDrop, Thermo Fisher Scientific, Waltham, MA, USA) with the protein specific



molecular weight (40 kDa) and extinction coefficient ( $30\,745\text{ M}^{-1}\cdot\text{cm}^{-1}$ ) as calculated using the ProtParam web service [29].

### Sodium dodecyl sulfate polyacrylamide gel electrophoresis

Molecular weight determination and purity assessment of protein samples was done by SDS/PAGE analysis [30]. Protein samples were separated by electrophoresis for 15 min at 100 V and 40 min at 200 V, and subsequently stained with Coomassie solution (10% (w/v) ammonium sulfate; 1.2% (v/v) phosphoric acid (85% aqueous solution), 0.1% Coomassie Brilliant Blue R250, 20% methanol) [31]. Visual documentation was carried out with an Advanced Imager system (INTAS Science Imaging Instruments GmbH, Goettingen, Germany).

### Measurement of esterase activity

4-nitrophenyl butyrate (*p*NPB) was used as a substrate for the determination of esterase activity as described before [28]. The enzyme reaction was composed of 100 nM enzyme in 100 mM potassium phosphate buffer pH 7.4, 1 mM *p*NPB, and 5% (v/v) acetonitrile. The reaction was monitored at 30 °C,  $\lambda = 410\text{ nm}$  in a microplate reader (SpectraMax i3x, Molecular Devices, LLC, Muenchen, Germany).

Effects of inhibitors were analyzed by determination of the esterase activity after 1-h incubation of about 100 nM protein at room temperature with 1 mM inhibitor, compared to a control reaction (100% activity) without addition of the inhibitor.

The optimal pH for PtEst1 activity was determined by endpoint measurements with *p*NPB as a substrate. The enzyme was diluted to 100 nM concentration with 10 mM potassium phosphate buffer pH 7.2; 5  $\mu\text{L}$  of the enzyme solution was mixed with 50  $\mu\text{L}$  Britton-Robinson buffer (40 mM acetic acid, 40 mM boric acid, 40 mM phosphoric acid, adjusted to the desired pH with NaOH), containing 1 mM *p*NPB, and 5% acetonitrile. The reaction mixture was incubated for 10 min at 30 °C. Then, 150  $\mu\text{L}$  Tris buffer (100 mM Tris pH 9) was added to the reaction mixture, and the absorption at 410 nm was measured subsequently with a microplate reader (SpectraMax i3x, Molecular Devices, LLC). The highest activity was set as 100%, and other activities were calculated in relation to the highest activity.

For thermostability assessment, 200 nM PtEst1 solution in 100 mM potassium phosphate buffer pH 7.4 was incubated in a PCR gradient cycler for 60 min at temperatures between 34 °C and 70.5 °C. Afterward, 10  $\mu\text{L}$  of the enzyme solution was used for the determination of residual esterase activity as described above. The lowest temperature (34 °C) was set as 100% activity, and residual activity at higher temperatures was calculated in relative to the lowest temperature.

For organic solvent tolerance assessment, 250  $\mu\text{L}$  200 nM PtEst1 solution in 100 mM potassium phosphate buffer pH 7.4 was combined with 250  $\mu\text{L}$  water supplemented with acetonitrile and methanol, respectively, to final concentrations of 10–30% and incubated for 96 h. Samples of 20  $\mu\text{L}$  of the organic solvent enzyme solution were taken after 1, 2, 3, 18, 24, 49, 72, and 96 h and used for the determination of residual activity as described above. The first sampling point was set as 100% activity, and subsequent sampling points were expressed relative to the initial activity.

### Substrate profiling assessment

Hydrolytic activity was assayed using a pH indicator assay at 550 nm using 96 structurally diverse esters in 384-well plates as previously described, with slight modifications [10,32]. Briefly, to 20  $\mu\text{L}$  of 5 mM 4-(2-Hydroxyethyl)-1-piperazine-propanesulfonic acid (EPPS) buffer (pH 8.0), 2  $\mu\text{L}$  of a stock ester solution was added to achieve a final concentration of  $10\text{ mg}\cdot\text{mL}^{-1}$  of each ester, to guarantee substrate saturation. Then, 20  $\mu\text{L}$  of 5 mM EPPS buffer pH 8.0 containing 0.95 mM Phenol Red was added. Buffer was dispensed with a QFill3 Microplate Filler (Genetix, San Francisco, CA, USA) and the buffers with a PRIMADIAG Demo liquid handling robot (EYOWN TECHNOLOGIES S.L., Madrid, Spain). Finally, 2  $\mu\text{L}$  of protein (from a  $1.0\text{ mg}\cdot\text{mL}^{-1}$  of cell extracts in 40 mM HEPES buffer pH 7.0) was immediately added to each well using an Eppendorf Repeater M4 pipette (Eppendorf, Hamburg, Germany). The total reaction volume was 44  $\mu\text{L}$ . Ester hydrolysis was measured at 30 °C in a Synergy HT Multi-Mode Microplate Reader (Izasa Scientific, Madrid, Spain) in continuous mode at 550 nm over 24 h. One unit (U) of enzyme activity was defined as the amount of free enzyme or enzyme bound to the carrier required to transform 1  $\mu\text{mol}$  of substrate in 1 min under the assay conditions using the reported extinction coefficient (Phenol red at 550 nm =  $8450\text{ M}^{-1}\cdot\text{cm}^{-1}$ ). All values, in triplicates, were corrected for nonenzymatic transformation.

The thermal melting point ( $T_{m50}$ ) of PtEst1 was determined by nanodifferential scanning fluorimetry (nanoDSF) with a Prometheus NT.Plex device (NanoTemper Technologies GmbH, Munich, Germany). The purified protein was mixed with organic solvent or buffer (100 mM potassium phosphate buffer pH 7.4) to reach 0 to 30% final concentration of organic solvent, and a final concentration of  $0.7\text{ mg}\cdot\text{mL}^{-1}$  of PtEst1 (ca.  $17.8\text{ }\mu\text{M}$ ). The mixture was subsequently loaded into capillary chips and assayed by nanoDSF, applying a linear heat ramp from 20 °C to 95 °C with a heat increment of  $1\text{ }^{\circ}\text{C}\cdot\text{min}^{-1}$ . Technical triplicates were done to analyze the mean and standard deviation of the melting temperature with the NANOTEMPER analysis software (NanoTemper Technologies GmbH, Munich, Germany). Experimental data were visualized using the GRAPHPAD PRISM software (San Diego, CA, USA).

## Crystallization

### Apoform PtEst1

Crystal screening was performed at 12 °C using the sitting drop vapor diffusion method. 0.1  $\mu$ L homogenous protein of PtEst1 (8.7 mg·mL<sup>-1</sup>, in 10 mM KPi buffer pH 7.2) was mixed with 0.1  $\mu$ L of the reservoir solution of commercial screens from NeXtal (Qiagen, Hilden, Germany) and Molecular Dimensions (Suffolk, UK) in 96-well plates (MRC3, SWISSCI AG, Zug, Switzerland) and equilibrated against 40  $\mu$ L. Little rods appeared after 21 to 115 days in 0.2 M magnesium chloride, 0.1 M MES pH 6.5, and 25% (w/v) PEG 4000 (PEG II, D11, NeXtal).

The crystallization condition was optimized by mixing 1  $\mu$ L protein (26.7 mg·mL<sup>-1</sup>) with 1  $\mu$ L reservoir solution and equilibrated against 300  $\mu$ L. After 3 days, needle clusters appeared in one well and were further optimized with the addition of additives (HR Additive Kit, Hampton Research, Aliso Viejo, CA, USA) or detergents (HR Detergent Kit, Hampton Research) by adding 0.2  $\mu$ L each drop. The most promising additives were TCEP hydrochloride, methanol, and sucrose monolaurate. In 0.25 M magnesium chloride, 0.1 M Tris pH 8.5, and 35% (w/v) PEG 4000 with 0.1 M TCEP, hydrochloride (end concentration 10 mM) crystals grew within 5–7 days and reached their maximum size of 320 × 80 × 60  $\mu$ m<sup>3</sup> after approximately 3–5 weeks. Harvesting was performed by carefully overlaying the crystal containing drops with 2  $\mu$ L mineral oil before the crystals were flash-frozen in liquid nitrogen.

### PtEst1 + Inhibitor (Methyl 4-methylumbelliferyl hexylphosphonate)

PtEst1 (26.7 mg·mL<sup>-1</sup>) was preincubated with the inhibitor methyl 4-methylumbelliferyl hexylphosphonate (end concentration 2 mM) on ice for at least 30 min. 0.3  $\mu$ L of homogenous protein was mixed with 0.2  $\mu$ L reservoir solution of the commercial screen PEG II of NeXtal (Qiagen) and 0.1  $\mu$ L of a 1 : 10 diluted seed stock of crashed crystals obtained from optimized apo enzyme and equilibrated against 40  $\mu$ L. The most promising crystals grew within 13 days in 0.2 M magnesium chloride, 0.1 M Tris pH 8.5, and 30% (w/v) PEG 4000 to a maximum size of 200 × 80 × 60  $\mu$ m<sup>3</sup> in a sitting drop plate (MRC3, SwisSCI) at 12 °C. The crystals were overlaid with mineral oil, harvested, and flash-frozen in liquid nitrogen.

### Data collection, processing, and structure determination

Crystals of the apo form of PtEst1 diffracted to a maximum of 1.35 Å. A dataset was collected at beamline P14 equipped with an the Eiger 16M detector at DESY (EMBL, Hamburg, Germany) at 100 K, processed with

XDS [33,34], and phased using the automated AUTORICK-SHAW pipeline (<http://www.embl-hamburg.de/Auto-Rickshaw/>) with only the PtEst1 protein sequence as input. The resulting initial model was subsequently auto-built using the ARP/WARP web service (<https://arpwarp.embl-hamburg.de>). After several rounds of model building using COOT [35] and subsequent refinement using REFMAC5 [36] from the CCP4 suite [37], the structure of the full-length PtEst1 protein was modeled into the electron density.

For the crystallographic analysis of PtEst1 in complex with the inhibitor, a high-resolution data set up to 1.81 Å was collected at ID29 equipped with an EIGER 4M detector (ESRF, Grenoble, France) at 100 K, processed with XDS and phased via molecular replacement using the PtEst1 apo structure determined before as search model. Model building and refinement was performed as described for the apo PtEst1 protein. The bound inhibitor and reaction products were manually fitted in the electron density. All data and refinement parameters are listed in Table 2. PtEst1 structures were deposited in the worldwide protein data bank (<https://www.rcsb.org>) under the accession codes 6Z68 (apo-PtEst1) and 6Z69 (PtEst1-inhibitor complex).

### Bioinformatic tools and software

Nucleotide and amino acid sequences were searched using NCBI BLAST [25]. For multiple sequence alignment, CLUSTAL OMEGA was used with default options [38]. To calculate the active site volume, all atoms but the main protein chain were omitted; the calculation was done with MOLE 2.0 [38], applying default settings and a 3.0 Å probe radius.

### Acknowledgements

We cordially acknowledge the staff of beamline P14 (DESY, EMBL, Hamburg, Germany) for their kind and helpful support during crystal screening and we are equally thankful to the staff of the ID29 beamline of the European Synchrotron Radiation Facility (Grenoble, France) for expertly providing synchrotron radiation facilities. The Center for Structural studies is funded by the DFG (grant number 417919780, INST 208/740-1 FUGG). The authors received funding from the European Union's Horizon 2020 Research and Innovation Programm ('Blue growth: unlocking the potential of seas and oceans') through the Project INMARE under grant agreement 634486. The work was furthermore part of the project LipoBiocat funded by the Federal Ministry of Education and Research under grant number 031B0837A. MF acknowledges grants PCIN-2017-078 (within the Marine Biotechnology ERA-NET), and BIO2017-85522-R and PID2019-106370RB-I00 grants from the Spanish Ministry of



Science and Innovation, Ministerio de Economía y Competitividad, Ministerio de Ciencia, Innovación y Universidades, Agencia Estatal de Investigación (AEI), Fondo Europeo de Desarrollo Regional (FEDER), and European Union (EU).

## Conflict of interest

The authors declare no conflict of interest.

## Author contributions

AH and SK performed the crystallization studies and collected the X-ray data. AH and SHJS refined the structure. AB and ST isolated, cloned, expressed and purified the protein, and performed the characterization studies. CC and MF contributed the analysis of the substrate fingerprint. SHJS and K-EJ supervised the study. All authors contributed to the writing of the manuscript.

## References

- 1 Jaeger KE & Eggert T (2002) Lipases for biotechnology. *Curr Opin Biotechnol* **13**, 390–397.
- 2 Arpigny JL & Jaeger KE (1999) Bacterial lipolytic enzymes: classification and properties. *Biochem J* **343** (Pt 1), 177–183.
- 3 Holmquist M (2000) Alpha/beta-hydrolase fold enzymes: structures, functions and mechanisms. *Curr Protein Pept Sci* **1**, 209–235.
- 4 Jaeger KE, Dijkstra BW & Reetz MT (1999) Bacterial biocatalysts: molecular biology, three-dimensional structures, and biotechnological applications of lipases. *Annu Rev Microbiol* **53**, 315–351.
- 5 Bauer TL, Buchholz PCF & Pleiss J (2020) The modular structure of alpha/beta-hydrolases. *FEBS J* **287**, 1035–1053.
- 6 Chen Y, Black DS & Reilly PJ (2016) Carboxylic ester hydrolases: classification and database derived from their primary, secondary, and tertiary structures. *Protein Sci* **25**, 1942–1953.
- 7 Khan FI, Lan D, Durrani R, Huan W, Zhao Z & Wang Y (2017) The lid domain in lipases: structural and functional determinant of enzymatic properties. *Front Bioeng Biotechnol* **5**, 16.
- 8 Li PY, Chen XL, Ji P, Li CY, Wang P, Zhang Y, Xie BB, Qin QL, Su HN, Zhou BC *et al.* (2015) Interdomain hydrophobic interactions modulate the thermostability of microbial esterases from the hormone-sensitive lipase family. *J Biol Chem* **290**, 11188–11198.
- 9 Ngo TD, Ryu BH, Ju H, Jang E, Park K, Kim KK & Kim TD (2013) Structural and functional analyses of a bacterial homologue of hormone-sensitive lipase from a metagenomic library. *Acta Crystallogr D* **69**, 1726–1737.
- 10 Martinez-Martinez M, Coscolin C, Santiago G, Chow J, Stogios PJ, Bargiela R, Gertler C, Navarro-Fernandez J, Bollinger A, Thies S *et al.* (2018) Determinants and prediction of esterase substrate promiscuity patterns. *ACS Chem Biol* **13**, 225–234.
- 11 Kovacic F, Babic N, Krauss U & Jaeger KE (2019) Classification of lipolytic enzymes from bacteria. In *Aerobic Utilization of Hydrocarbons, Oils and Lipids* (Rojo F, ed.) pp. 1–35. Springer International, Cham, Switzerland.
- 12 Andersen KR, Leksa NC & Schwartz TU (2013) Optimized *E. coli* expression strain LOBSTR eliminates common contaminants from His-tag purification. *Proteins* **81**, 1857–1861.
- 13 Ferrer M, Bargiela R, Martinez-Martinez M, Mir J, Koch R, Golyshina OV & Golyshin PN (2015) Biodiversity for biocatalysis: a review of the  $\alpha/\beta$ -hydrolase fold superfamily of esterases-lipases discovered in metagenomes. *Biocatal Biotransform* **33**, 235–249.
- 14 Magnusson AO, Rotticci-Mulder JC, Santagostino A & Hult K (2005) Creating space for large secondary alcohols by rational redesign of *Candida antarctica* lipase B. *ChemBioChem* **6**, 1051–1056.
- 15 Kraut J (1977) Serine proteases: structure and mechanism of catalysis. *Annu Rev Biochem* **46**, 331–358.
- 16 Shang F, Lan J, Liu W, Chen Y, Wang L, Zhao J, Chen J, Gao P, Ha NC, Quan C *et al.* (2019) Structural and functional analyses of the lipase CinB from *Enterobacter asburiae*. *Biochem Biophys Res Commun* **519**, 274–279.
- 17 Yang S, Qin Z, Duan X, Yan Q & Jiang Z (2015) Structural insights into the substrate specificity of two esterases from the thermophilic *Rhizomucor miehei*. *J Lipid Res* **56**, 1616–1624.
- 18 Schiefner A, Gerber K, Brosig A & Boos W (2014) Structural and mutational analyses of Aes, an inhibitor of MalT in *Escherichia coli*. *Proteins* **82**, 268–277.
- 19 Inoue D, Tsunoda T, Sawada K, Yamamoto N, Saito Y, Sei K & Ike M (2016) 1,4-Dioxane degradation potential of members of the genera *Pseudonocardia* and *Rhodococcus*. *Biodegradation* **27**, 277–286.
- 20 Singhvi P, Saneja A, Srichandan S & Panda AK (2020) Bacterial inclusion bodies: a treasure trove of bioactive proteins. *Trends Biotechnol* **38**, 474–486.
- 21 Troeschel SC, Drepper T, Leggewie C, Streit WR & Jaeger KE (2010) Novel tools for the functional expression of metagenomic DNA. *Methods Mol Biol* **668**, 117–139.
- 22 Bollinger A, Molitor R, Thies S, Koch R, Coscolin C, Ferrer M & Jaeger KE (2020) Organic-solvent-tolerant carboxylic ester hydrolases for organic synthesis. *Appl Environ Microbiol* **86**, e00106-20.

- 23 Reyes-Duarte D, Ferrer M & Garcia-Arellano H (2012) Functional-based screening methods for lipases, esterases, and phospholipases in metagenomic libraries. *Methods Mol Biol* **861**, 101–113.
- 24 Nolasco-Soria H, Moyano-Lopez F, Vega-Villasante F, Del Monte-Martinez A, Espinosa-Chaurand D, Gisbert E & Nolasco-Alzaga HR (2018) Lipase and phospholipase activity methods for marine organisms. *Methods Mol Biol* **1835**, 139–167.
- 25 Wheeler DL, Church DM, Federhen S, Lash AE, Madden TL, Pontius JU, Schuler GD, Schriml LM, Sequeira E, Tatusova TA *et al.* (2003) Database resources of the National Center for Biotechnology. *Nucleic Acids Res* **31**, 28–33.
- 26 Green MR & Sambrook J (2012) Molecular Cloning: A Laboratory Manual. Cold Spring Harbor Laboratory Press, Cold Spring Harbor, NY.
- 27 Woodcock DM, Crowther PJ, Doherty J, Jefferson S, DeCruz E, Noyer-Weidner M, Smith SS, Michael MZ & Graham MW (1989) Quantitative evaluation of *Escherichia coli* host strains for tolerance to cytosine methylation in plasmid and phage recombinants. *Nucleic Acids Res* **17**, 3469–3478.
- 28 Bollinger A, Thies S, Knieps-Grunhagen E, Gertzen C, Kobus S, Hoppner A, Ferrer M, Gohlke H, Smits SHJ & Jaeger KE (2020) A novel polyester hydrolase from the marine bacterium *Pseudomonas aestusnigri* – structural and functional insights. *Front Microbiol* **11**, 114.
- 29 Gasteiger E, Hoogland C, Gattiker A, Duyaund S, Wilkins MR & Appel RD. (2005) Protein identification and analysis tools on the ExPASy serve. In *The Proteomics Protocols Handbook* (Walker JM, ed.), pp. 571–607. Humana Press, Totowa, NJ.
- 30 Laemmli UK (1970) Cleavage of structural proteins during the assembly of the head of bacteriophage T4. *Nature* **227**, 680–685.
- 31 Blakesley RW & Boezi JA (1977) A new staining technique for proteins in polyacrylamide gels using coomassie brilliant blue G250. *Anal Biochem* **82**, 580–582.
- 32 Reyes-Duarte D, Coscolin C, Martinez-Martinez M, Ferrer M & Garcia-Arellano H (2018) Functional-based screening methods for detecting esterase and lipase activity against multiple substrates. *Methods Mol Biol* **1835**, 109–117.
- 33 Kabsch W (2010) XDS. *Acta Crystallogr D* **66**, 125–132.
- 34 Kabsch W (2010) Integration, scaling, space-group assignment and post-refinement. *Acta Crystallogr D* **66**, 133–144.
- 35 Emsley P & Cowtan K (2004) Coot: model-building tools for molecular graphics. *Acta Crystallogr D* **60**, 2126–2132.
- 36 Murshudov GN, Skubak P, Lebedev AA, Pannu NS, Steiner RA, Nicholls RA, Winn MD, Long F & Vagin AA (2011) REFMAC5 for the refinement of macromolecular crystal structures. *Acta Crystallogr D* **67**, 355–367.
- 37 Collaborative Computational Project, N (1994) The CCP4 suite: programs for protein crystallography. *Acta Crystallogr D* **50**, 760–763.
- 38 Sievers F, Wilm A, Dineen D, Gibson TJ, Karplus K, Li W, Lopez R, McWilliam H, Remmert M, Soding J *et al.* (2011) Fast, scalable generation of high-quality protein multiple sequence alignments using Clustal Omega. *Mol Syst Biol* **7**, 539.